NANO LETTERS

pubs.acs.org/NanoLett

Letter

Near-Field Imaging and Time-Domain Dynamics of Photonic Topological Edge States in Plasmonic Nanochains

Qiuchen Yan, En Cao, Quan Sun,* Yutian Ao, Xiaoyong Hu,* Xu Shi, Qihuang Gong, and Hiroaki Misawa*

Cite This: https://doi.org/10.1021/acs.nanolett.1c03324

Read Online

ACCESS | Metrics & More | Article Recommendations | Supporting Information

ABSTRACT: Time-domain dynamic evolution properties of topological states play an important role in both fundamental physics study and practical applications of topological photonics. However, owing to the absence of available ultrafast time-domain dynamic characterization methods, studies have mostly focused on the frequency-domain-based properties, and there are few reports demonstrating the time-domain-based properties. Here, we measured the dynamic near-field responses of plasmonic topological structures of gold nanochains with the configuration of the Su−Schrieffer−Heeger model by using ultrahigh spatial-temporal resolution photoemission electron microscopy. The dephasing time of plasmonic topological edge states increases with increasing the bulk lattice number that has a threshold requirement and finally reaches saturation. We directly revealed through simulation that there is a transient bulk state in the evolution of topological edge states, that is, the energy undergoes relaxation from oscillation between the bulk lattice and the edge. This work shows a new perspective of time-domain dynamic topological photonics.

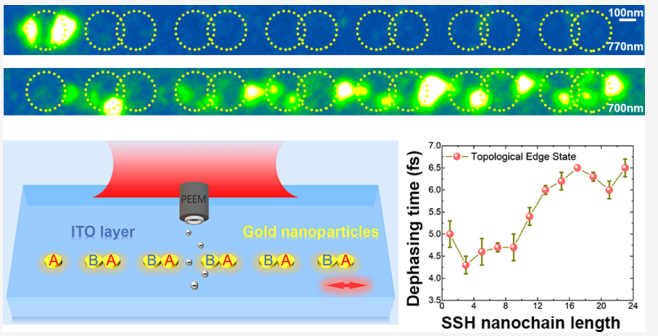

KEYWORDS: *topological photonics, plasmonic nanochain, photoemission electron microscopy, ultrafast optics, nanofemto scale*

Topology provides a new degree of freedom for photons, which can be used as a variable in nanophotonic systems, similar to frequency, wave vector, polarization and phase.[1] Topological photonics is one of the research frontiers of nanophotonics and nanotechnology. Many different studies have been performed in topological photonics, such as on non-Hermitian topological systems,[2] quantum topological photonics,[3] and high-dimensional topological photonics.[4] To date, the band topology emerged as a mathematical tool in understanding fundamental properties of topological photonics,[1,5] and the research on topological photonics has mostly focused on the frequency domain for various topological photonic structures, including topological photonic crystals,[6] resonance ring arrays,[7] and topological metamaterials.[8] These studies have improved the applications of topological photonics in optical devices, such as topological lasers[9,10] and topological quantum sources.[11] The time-domain-based responses of topological states can also have potential novel physical effects and significant applications.[12] Fan's, Brandes', and Theocharis's groups reported the change of the topological orders under intensity-dependence nonlinear modulation.[13−15] Agarwal's group observed the transmission properties of topological waveguides.[16] Segev's group proposed a concept of topological photonic time crystals.[17] Spielman's group reported a direct imaging method of topological edge states in cold-atom systems.[18] Sentef's group found that the polaritonic states in a ribbon geometry were selectively resonant excited by using time- and angle-resolved photoluminescence technology.[19] As a consequence, it is necessary and important to study the time-domain response of topological states. However, there are few reports on studying the ultrafast time-domain dynamic response of topological states, because it needs combination of ultrafast time-resolved technology and ultrahigh space-resolved technology.

Here, the time-domain dynamics evolution of topological edge states (TESs) in gold nanochains with the configuration of the Su−Schrieffer−Heeger (SSH) model are revealed by using ultrahigh spatial-temporal resolution photoemission electron microscopy (PEEM), which is from a new perspective in time-domain topological photonics. As is known, the localized surface plasmonic TESs have been reported and experimentally realized.[20] In addition, the plasmonic nanochains also have been studied for years, including the near-field and the far-field properties of the interaction between nanoparticles,[21−23] the nanochain energy transport,[24,25] the

Received: August 27, 2021
Revised: September 26, 2021

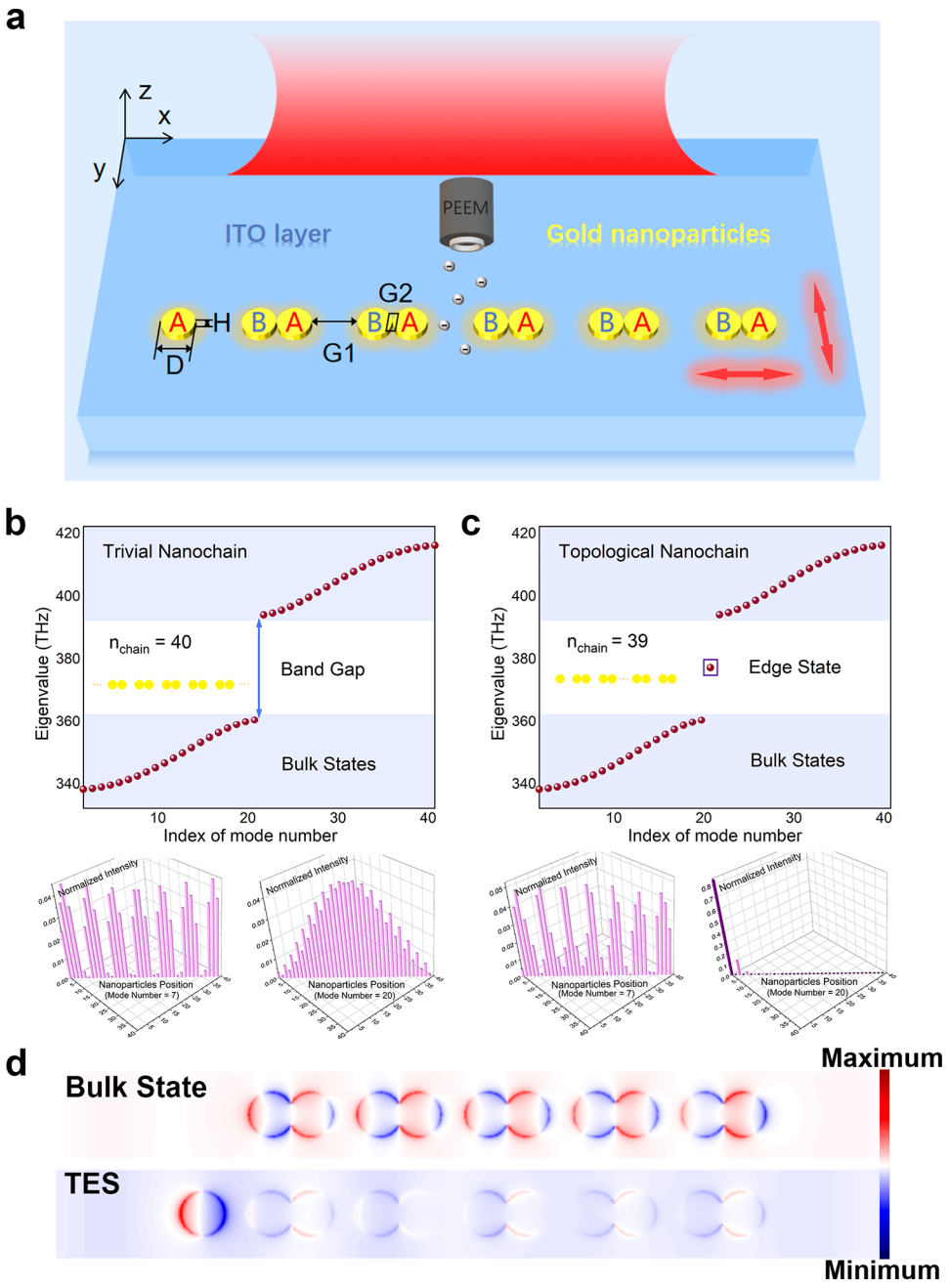

Figure 1. (a) Three-dimensional schematic structure of the plasmonic SSH nanochain. D, H, G_1, and G_2 represent the nanoparticle diameter, height, long gap distance and overlapping distance, respectively. A and B represent the different positions of nanoparticles in a unit. An ITO layer is the substrate, and gold nanoparticles are fabricated on it. The red arrow with the direction parallel to the x-axis indicates L-polarized incident light, and the red arrow with the direction parallel to the y axis indicates T-polarized incident light. (b,c) Calculation of the energy eigenvalues in two cases of a trivial dimer nanochain and a plasmonic SSH nanochain with an isolated nanoparticle on the left terminal side. The insets show the field distributions of different states. (d) Simulated charge distributions of a trivial dimer nanochain and a plasmonic SSH nanochain with an isolated nanoparticle on the left terminal side.

topological photonic nanochains with retardation and radiative effects,[26,27] and coherent temporal plasmonics.[28] Therefore, we consider the plasmonic SSH nanochains as the basic structures, and the nanochain length, that is, the bulk lattice size, can be changed by increasing the number of nanoparticles. The direct evolution process of plasmonics is extremely quick; consequently, to indicate this dynamic process and to reveal the fundamental evolution regulation of TESs we obtained the responses of SSH nanochains with different lengths.

The TES dephasing time of each SSH nanochain can be obtained by PEEM,[29,30] through our dynamic measurement of the nanochain length dependence under longitudinally (L) polarized excitation, we find that the dephasing time of plasmonic TESs first increases as the nanochain length increases and then reaches saturation. This result clearly shows that during the TES evolution process, there is coupling between the bulk lattices and the edges, and the coupling affects the TESs dephasing time. In other words, the TESs dephasing time varies with the bulk lattices, and the bulk

https://doi.org/10.1021/acs.nanolett.1c03324
Nano Lett. XXXX, XXX, XXX−XXX

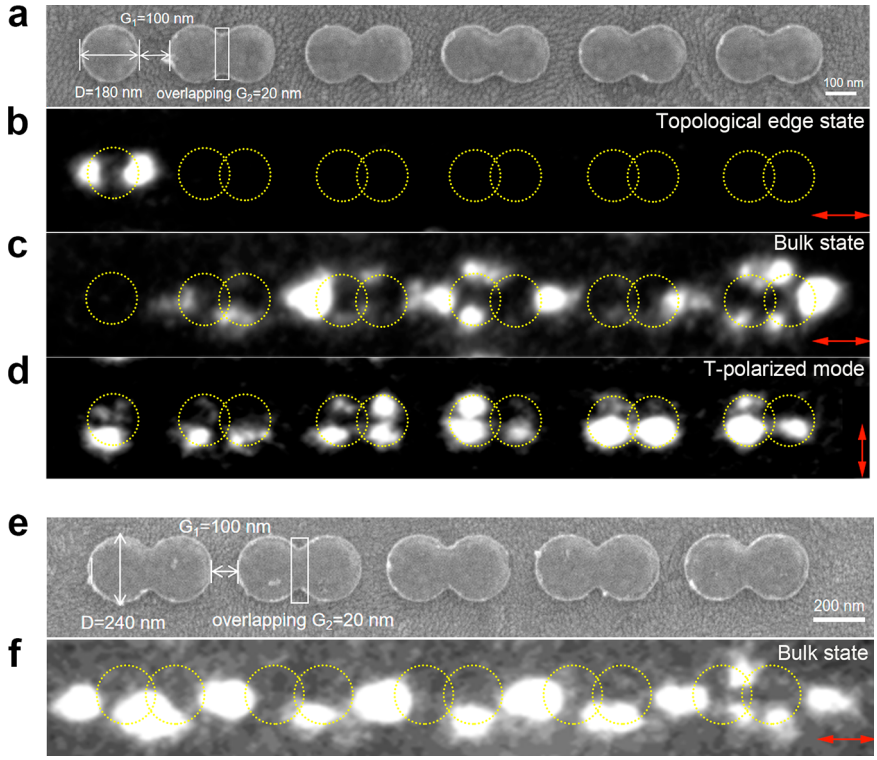

Figure 2. (a) SEM image of gold nanoparticles arrayed as plasmonic SSH nanochains with a nanoparticle diameter of 180 nm, G_1 of 100 nm and overlapping G_2 of 20 nm. (b)-(d) Near-field imaging of TESs and bulk states under L-polarized incident light with wavelengths of 770 and 700 nm and the T-polarized mode under T-polarized incident light with a wavelength of 750 nm. The dotted yellow circles indicate the spatial positions of the SSH nanochain. (e) SEM image of gold nanoparticles arrayed as a trivial dimer nanochain with a nanoparticle diameter of 240 nm, G_1 of 100 nm and overlapping G_2 of 20 nm. (f) Near-field imaging of the trivial nanochain under L-polarized incident light with an excitation wavelength of 800 nm.

lattices are involved in and contribute to the evolution of TESs in time domain. Moreover, there is a threshold requirement of the bulk lattice number for the formation of stable TESs. This phenomenon is not found in trivial nanochains without TESs or in the case of localized surface plasmonic modes excited under transversely (T) polarized excitation. Furthermore, we simulate the evolution process of TESs by Lumerical FDTD Solutions with single-wavelength light source in the corresponding band gap, obtaining a movie that directly demonstrates the evolution process of plasmonic TESs in the time domain, that is, the plasmonic energy undergoes relaxation from oscillation between the bulk lattice and the edge, subsequently tending to dephase, which well supports the experimental conclusion. This work opens up the new research field of time-domain dynamic topological photonics.

THEORETICAL ANALYSIS OF THE GENERATION OF TESS IN SSH PLASMONIC NANOCHAINS

A gold nanoparticle array was used to construct the one-dimensional (1D) plasmonic SSH nanochains. By using the tight-binding model, the Hamiltonian of the SSH model could be simplified as follows[31]

$$\hat{H} = v\sum_{m=1}^{n}(|m, B><m, A| + h.c.) + w\sum_{m=1}^{n-1}(|m+1, A><m, B| + h.c.) \quad (1)$$

In eq 1, n represents the total number of units of the SSH nanochain, m is the position number, and v and w represent the coupling strengths between intra- and interunits, respectively; TESs only exist when $v < w$. The gold nanoparticles, according to the v and w coupling law, are arranged as an SSH nanochain extending along the direction of L-polarized incident light, as shown in Figure 1a. When the diameter D of the gold nanoparticles is given, the coupling strength Ω between two gold nanoparticles is inversely proportional to the third power of the distance G[26]

$$\Omega = \frac{\omega_0}{2}\left(\frac{D}{2G}\right)^3 \quad (2)$$

where w_0 represents the energy eigenvalue of an isolated nanoparticle. When the distance G_1 between the nanoparticles is large, the coupling strength between the two nanoparticles is weak. In contrast, when the distance between the nanoparticles is very small, a strong electric field intensity will occur in the small gap because of the strong coupling strength between the two nanoparticles. However, the tight-binding approximation is invalid in the strong coupling region. Thus, we used overlapping gold nanoparticles as interunits in our work to avoid a strong interaction field. The interunit nanoparticles overlap by a distance G_2, which does not produce a strong gap field, and there can be a stronger interaction than in the case of intraunits.[32] By analyzing a two-level system, the relative quantity of coupling strength can be obtained from the offset of the resonance frequency. In the case of overlapping-gap nanoparticles, the offset is obviously larger than the case of

https://doi.org/10.1021/acs.nanolett.1c03324
Nano Lett. XXXX, XXX, XXX−XXX

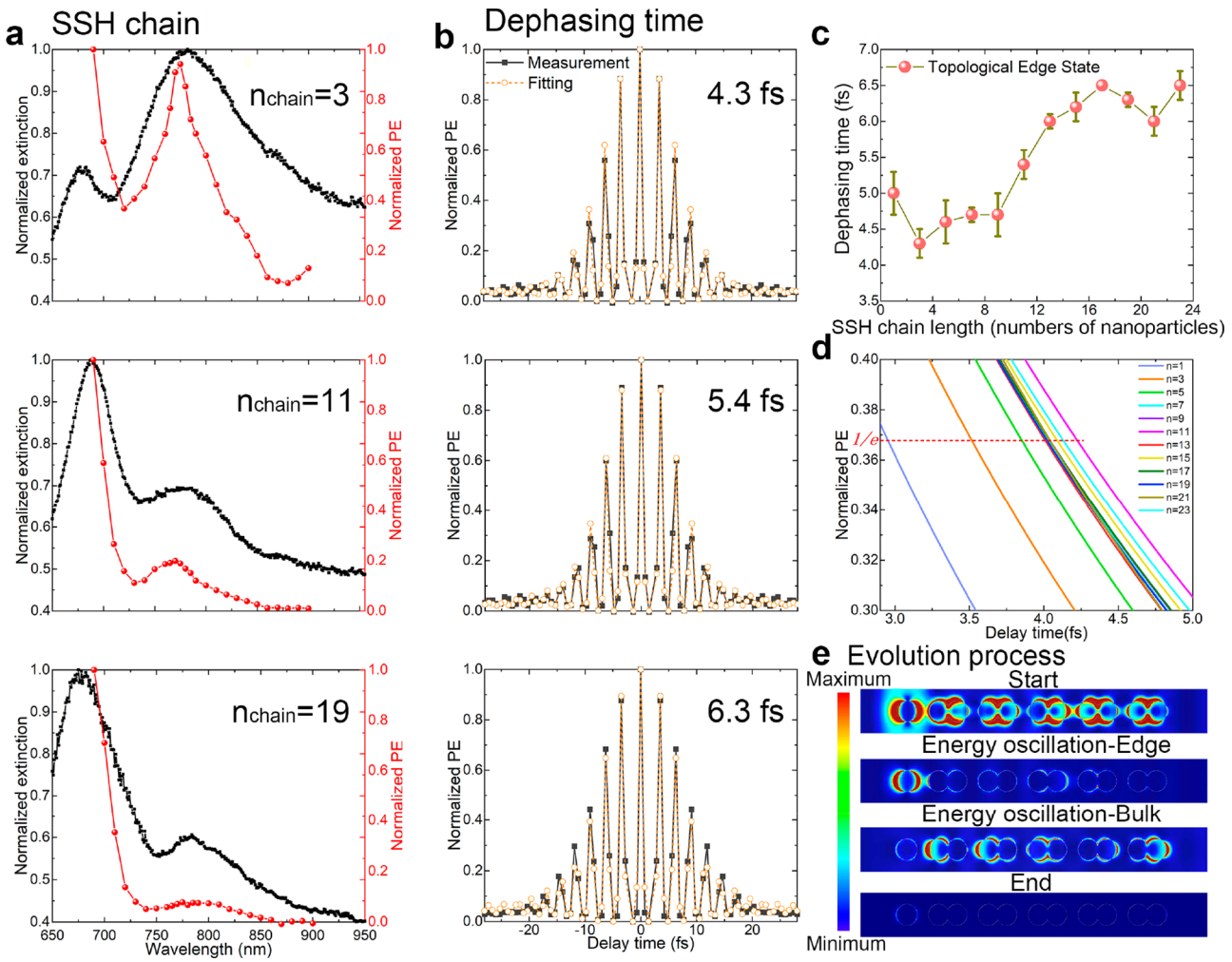

Figure 3. (a) Experimental far-field normalized extinction and near-field normalized PE intensity spectra of plasmonic SSH nanochains with different nanoparticle numbers of n = 3, n = 11, and n = 19. The nanoparticle diameter is 180 nm. The black lines represent far-field spectra, and the red lines represent near-field spectra. (b) Experimental dephasing time of SSH nanochain TESs with different nanoparticle numbers of n = 3, n = 11, and n = 19. The nanoparticle diameter is 180 nm. The solid lines are the measurement data, and the dashed lines are the fitting results of the measurement data. (c) Length-dependent curve of the changing dephasing time for plasmonic SSH nanochains. Small short green lines represent the fitting errors. (d) Simulated lifetime change of the TES under different plasmonic SSH nanochain lengths, which are obtained by using the delay time corresponding to e^{-1} of the highest intensity at the zero point. This shows an enlarged part of the delay time from 2.9 to 5.0 fs. (e) Screenshots of the TES evolution dynamic process at different times.

nontouching nanoparticles when they are under the same physical mode. A detailed explanation is provided in Supporting Information I. Therefore, this configuration meets the requirements of the SSH model, which can generate the TESs.

Indium tin oxide (ITO)-coated glass was used as the substrate, and gold was used as the material for nanoparticles with a diameter of 180 nm and a height of 30 nm. First, to determine the energy eigenvalue of an isolated nanoparticle, we obtained the energy eigenvalue w_0 from simulation based on its extinction spectrum and near-field spectrum through the finite-difference time-domain method (Lumerical FDTD Solutions). Second, we calculated the mode distribution of energy eigenvalues for SSH configuration under L-polarized excitation. Specifically, when the coupling strength of intraunits v was greater than that of interunits w, this nanochain was a trivial 1D photonic crystal, which was also called a trivial dimer nanochain with an energy band gap.[31] There was no eigenvalue distribution in the band gap, as shown in Figure 1b. In contrast, when the coupling strength between intraunits v was less than that between interunits w, there was one isolated eigenvalue distribution in the band gap, that is, TES, and this configuration was a topological nanochain. The field intensity distribution could be verified by the simulated results shown in Figure 1c. Similarly, there were two degenerate eigenvalues in the band gap as shown in Figure S4 where the nanochain had two TESs. However, there would be no TES in this configuration if it was under the excitation of T-polarized incident light, because the coupling strength between intra-units v and the interunits w was almost equal. Moreover, we simulated the charge distributions of a trivial dimer nanochain with bulk state and a plasmonic SSH nanochain with TES shown in Figure 1d.

NEAR-FIELD IMAGING OF TESS IN SSH PLASMONIC NANOCHAINS

The near-field imaging and the time-domain dynamic response of plasmonic topological SSH nanochains was obtained by using time-resolved PEEM (TR-PEEM). TR-PEEM is a

https://doi.org/10.1021/acs.nanolett.1c03324
Nano Lett. XXXX, XXX, XXX−XXX

technique with both ultrahigh time and ultrahigh spatial resolution.[33] It can be used to simultaneously observe the near-field mode distribution and measure the plasmonic dephasing time with ultrashort laser pulses,[34,35] which is very beneficial for measuring the ultrafast dynamic process of plasmonic TESs. Details of the PEEM measurement system can be found in the Supporting Information V. We fabricated the samples by using electron beam lithography, and the detailed fabrication process is described in the Supporting Information III. A scanning electron microscopy (SEM) image of a plasmonic topological SSH nanochain is shown in Figure 2a. The long distance between the nanoparticles, which represents the intraunit coupling strength v, was 100 nm, and the overlapping distance, which represents the interunit coupling strength w, was 20 nm. The overlapping distance was chosen from the measured far-field spectra shown in S5, which demonstrates a series of extinction spectra with different overlapping distances. When the overlapping distance is 20 nm, the peak wavelength of the TESs is approximately 780 nm, which is appropriate for experiments because it is close to the 800 nm central wavelength of the laser source. As is known, summarizing the regulation of the time-domain dynamic response of a topological configuration using only one nanostructure is difficult; therefore, we designed a series of nanochains with different structural bulk sizes to study this dynamic process. The change in the nanochain bulk size was reflected in the continuous increase in the nanochain length, from $n = 1$ to $n = 23$ with an interval of $\Delta n = 2$. More SEM images of nanochains of different lengths are shown in Supporting Information IV. Moreover, as shown in Figure 2e, we fabricated trivial dimer nanochains for reference with different nanochain lengths from $n = 4$ to $n = 22$ with an interval of $\Delta n = 6$, and the diameter of the nanoparticles forming the trivial nanochains was 240 nm, which is appropriate for experiments with a bulk state peak wavelength of 800 nm.

Subsequently, we experimentally measured the extinction spectra of these structures with different nanochain lengths in the far field and then placed these structures into the PEEM instrument for measurement to obtain the near-field mode distribution and spectra. The plasmonic mode distributions of an SSH nanochain under L-polarized incident light are shown in Figure 2b,c, which represent the topological edge mode with an excitation wavelength of 770 nm and the bulk mode with an excitation wavelength of 700 nm, respectively. The arrows indicate the direction of L-polarized excitation. The plasmonic mode distribution of the SSH nanochain under T-polarized incident light with an excitation wavelength of 750 nm is shown in Figure 2d, and the arrow indicates the direction of T-polarized excitation. In addition, the plasmonic mode distribution of the trivial dimer nanochain under L-polarized incident light with an excitation wavelength of 800 nm is shown in Figure 2f. There was no change in the bulk mode distribution throughout the measured wavelength range, indicating that no TES existed in the trivial dimer nanochain.

The far-field extinction spectra and the near-field spectra are shown in Figure 3a. We selected three typical cases of different plasmonic SSH nanochain lengths, that is, $n = 3$, $n = 11$, and $n = 19$, which corresponds to an increase in the nanochain bulk size. In our experiments, there were slight peak wavelength differences for TESs in near-field spectra with peak wavelengths of 770 nm and in far-field spectra with peak wavelengths of 780 nm because of fabrication errors and different plasmonic properties in the near field and far field.

TIME-DOMAIN DYNAMICS OF TESS IN SSH PLASMONIC NANOCHAINS

We further used ultrashort 7 fs laser pulses to measure the time-domain dynamic response of plasmonic TESs after determining the near-field peak wavelength and mode distribution of the plasmonic SSH nanochains. We obtained experimental data of the dephasing time by using a Mach–Zehnder interferometer instrument. The dephasing time represents the lifetime of plasmonic modes, and a long lifetime is beneficial for the interaction between light and matter and low loss. In our work, we obtained different dephasing times to reflect the discrepancies in TESs for different plasmonic topological SSH nanochain lengths. We selected the area in which only TESs exist to obtain accurate dephasing time data, as detailed in Figures S9 and S10. The results of the plasmonic SSH chain dephasing time with $n = 3$, $n = 11$, and $n = 19$ is shown in Figure 3b. The dephasing time changed with increasing nanochain bulk size. For the case of $n = 3$, the TES dephasing time was only 4.3 fs. For the case of $n = 11$, the dephasing time increased to 5.4 fs. For the case of $n = 19$, the dephasing time increased to 6.3 fs. To study the influence of the bulk lattice number on the formation of robust topological states in detail, we also measured the relationship between the bulk lattice number and the dephasing time of TESs in other topologically nontrivial plasmonic SSH nanochains, and the measured results are shown in Figure 3c. As a consequence of the disorders generated from nanofabrication, there can be different photon emission responses when measuring and cause some fluctuations in the measured dephasing time. The dephasing time began at approximately 5.0 fs, corresponding to that of localized plasmonic resonance of a single nanoparticle at the same wavelength. Subsequently, the dephasing time became longer with increasing n, and it rapidly grew when the nanoparticle number n increased from 9 to 13. When the nanoparticle number n was over 13, the dephasing time of TESs reached saturation around 6.5 fs without obvious changes, that is, the dephasing time oscillated between 6 and 6.5 fs as the nanochain length continued to increase. This oscillation phenomenon sufficiently indicates that the dephasing time of the TESs has reached saturation at this time, and increasing the nanochain length has no effect on the dephasing time after $n = 13$. This illustrates that there is a threshold requirement of the bulk lattice number, that is, the bulk size, for the evolution of TESs. Under the same experimental conditions, we also measured the TES dephasing time in the case of plasmonic SSH nanochains with overlapping G_2 of 10 nm, which led to the same conclusion as above. These additional results are shown in Supporting Information VIII.

In addition, we numerically studied the change on the dephasing time of the TES with number of the unit cells in the SSH nanochains by using single-wavelength in corresponding band gap, and the results are shown in Figure 3d, which are in good agreement with the experimental conclusion. The simulation was performed under nanochain lengths ranging from $n = 1$ to $n = 23$ with the SSH configuration, and we regarded the delay time corresponding to e^{-1} of the highest intensity at the zero point as the lifetime of the TES. This shows an enlarged part of the delay time from 2.9 to 5.0 fs, which clearly indicates the lifetime of the TES for each nanochain length, and the complete numerical results are provided in the Figure S15c. This also illustrates that the TES dephasing time first rapidly increases and then saturates with

https://doi.org/10.1021/acs.nanolett.1c03324
Nano Lett. XXXX, XXX, XXX−XXX

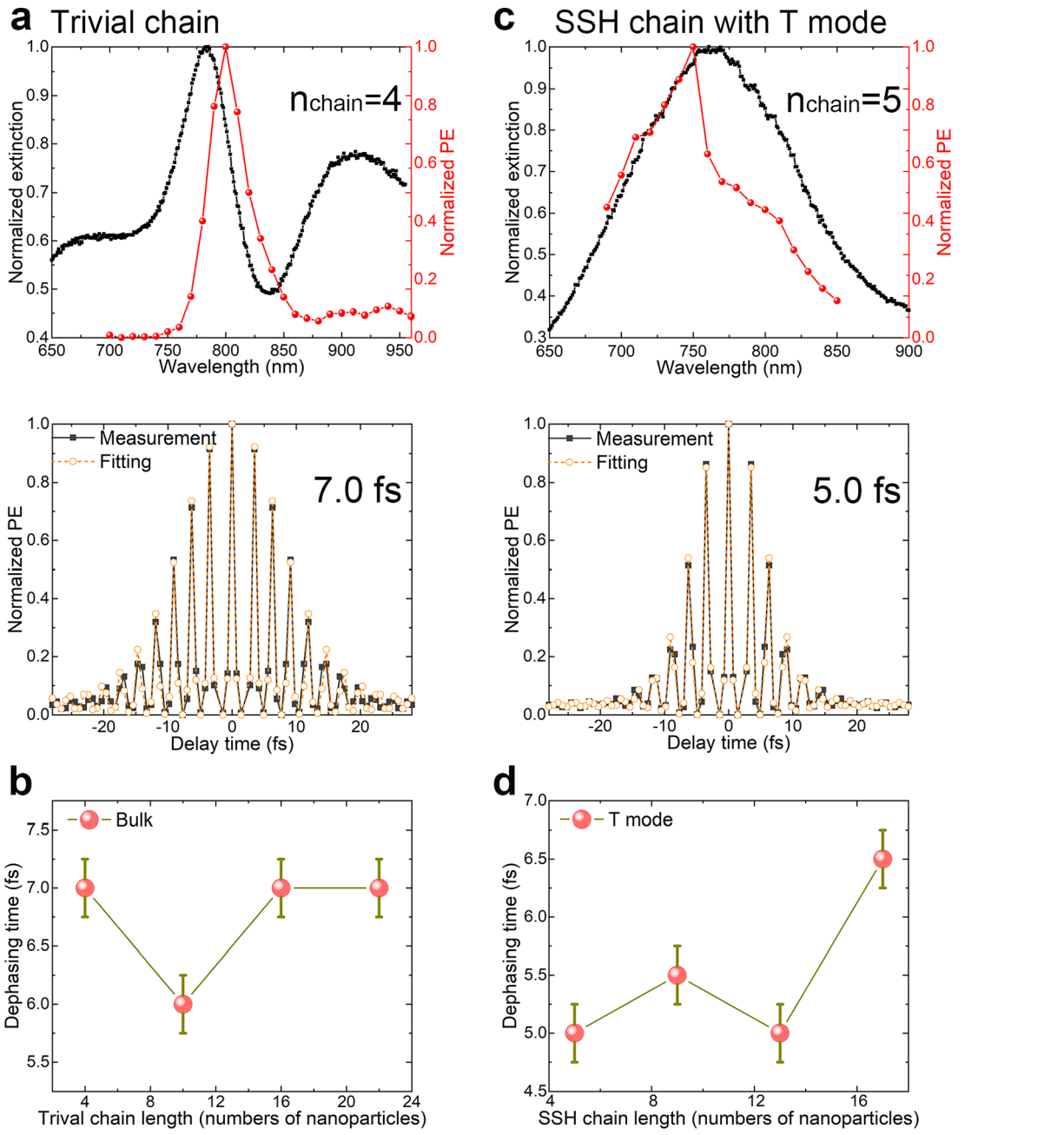

Figure 4. (a) Experimental far-field normalized extinction and near-field normalized PE intensity spectra of a trivial nanochain with a nanochain length of $n = 4$, and its experimental dephasing time of trivial bulk states. The nanoparticle diameter is 240 nm. (b) Length-dependent curve of the changing dephasing time for trivial nanochains. The fitting errors are represented by the small short green lines. (c) Experimental far-field extinction and near-field normalized PE intensity of an SSH nanochain with a nanochain length of $n = 5$, and its experimental dephasing time for the plasmonic T mode excited by T-polarized incident light. The nanoparticle diameter is 180 nm. (d) Length-dependent curve of the changing dephasing time for the plasmonic T mode of SSH nanochains. Small short green lines represent the fitting errors.

increasing the nanochain length. To explain how the nanochain length affects the dephasing time of TESs, we provide Movie M1 in Supporting Information XI, which can directly show the dynamic evolution process of TESs. We took four screenshots of different important moments during the dynamic process, as shown in Figure 3e. When the plasmonic SSH nanochains were excited by L-polarized incident light, plasmonic modes were initially excited over all nanoparticles. Then, energy oscillation occurred between the bulk lattice and the edge. Finally, the oscillation decreased, and the TESs continued dephasing. This process indicates that the evolution of TESs is related to the bulk lattice and that there is a transient bulk state in the time domain. Therefore, the nanochain bulk size affects the TESs, and the bulk lattices are involved in and contribute to the evolution of TESs in time domain.

It can also be explained by the mechanism of the dephasing time of the edge state. It is reported that the dephasing time is related to the loss of the metal, and the absorption cross section and scattering cross section can represent ohmic loss and radiation loss, respectively.[36,37] We concluded from simulating that the dephasing time of the edge state is mainly

https://doi.org/10.1021/acs.nanolett.1c03324
Nano Lett. XXXX, XXX, XXX−XXX

influenced by the radiative loss and the ohmic loss of the metal mainly affect the bulk dimers. A detailed description can be found in Supporting Information IX.

NEAR-FIELD AND TIME-DOMAIN DYNAMIC RESPONSE IN TRIVIAL NANOCHAINS

Moreover, to prove that the above-mentioned dynamic tendency of the TES dephasing time is a unique characteristic of topological systems we also measured the extinction spectra and the near-field spectra, obtaining the dephasing time in the case of trivial dimer nanochains for reference. We tuned the nanoparticle diameter to 240 nm to obtain bulk-state peak wavelengths of 800 nm. Figure 4a displays the case of $n = 4$. Subsequently, we selected the areas of bulk states in different nanochains and fitted the dephasing time. The nanochain length-dependent curve of the bulk state dephasing time, shown in Figure 4b, indicates an irregular change in the dephasing time with increasing nanochain length from $n = 4$ to $n = 22$. This proves that the topological configurations have the unique characteristic of the time-domain dynamic response. Furthermore, we performed the same experimental operations to measure plasmonic nontrivial SSH nanochains under T-polarized incident light, which is another kind of trivial nanochain. There was no TES when the nanochain was under T-polarized excitation. Figure 4c demonstrates the extinction spectra and near-field spectra with a peak wavelength of 750 nm in the case of $n = 5$, and the dephasing time was 5.0 fs. The nanochain length-dependent curve of the T-mode dephasing time displayed in Figure 4d shows an irregular change in the dephasing time with increasing nanochain length. This proves that the TES contributes to the dephasing time change under L-polarized excitation with the nontrivial SSH configuration.

CONCLUSION

Because of the ultrafast decay process of plasmonic modes in gold nanoparticles, we cannot directly observe the evolution process of the TESs. However, by measuring the dephasing time of SSH nanochains with different nanochain lengths, we conclude that the dephasing time of TESs increases as the nanochain bulk size increases and finally reaches saturation. Here, we regard the nanochain length as the nanochain bulk size. In other words, the bulk lattice plays a significant role in the evolution process of TESs in time domain. We can understand it from another aspect that when the bulk and the edges are excited simultaneously the TESs are not formed all at once but through the bulk energy and the edge energy oscillation in time domain, while there is only TESs mode distribution reflected in the frequency domain. Moreover, the threshold requirement for TES dephasing time is of vital importance and is helpful for us to understand the evolution essence of TESs. It can be expanded to other topological configurations or dimensions in the future. Our work not only paves the way for the fundamental study of time-domain topological photonics but also promotes the realization of novel topological photonic devices.

ASSOCIATED CONTENT

Supporting Information

The Supporting Information is available free of charge at https://pubs.acs.org/doi/10.1021/acs.nanolett.1c03324.

Theory of overlapping-dimer SSH nanochain, methods of sample fabrication, experimental measurements, as well as numerical simulation of plasmonic nanochains with different lengths; near-field images under different wavelength excitation and time-resolved measurements of SSH nanochains with different parameters of diameter and overlapping gaps; additional spectra and figures (PDF)

Movie of simulated evolution process of TES under single-wavelength excitation light (AVI)

Movie of dephasing time measurement of specific-length SSH nanochains with diameter of 180 nm (AVI)

Movie of dephasing time measurement of specific-length SSH nanochains with diameter of 240 nm (AVI)

AUTHOR INFORMATION

Corresponding Authors

Quan Sun − *Yangtze Delta Institute of Optoelectronics, Peking University, Nantong, Jiangsu 226010, P.R. China;* orcid.org/0000-0001-5413-8038; Email: sunquan@ydioe.pku.edu.cn

Xiaoyong Hu − *State Key Laboratory for Mesoscopic Physics and Department of Physics, Collaborative Innovation Center of Quantum Matter and Frontiers Science Center for Nano-optoelectronics, Beijing Academy of Quantum Information Sciences, Peking University, Beijing 100871, P.R. China; Yangtze Delta Institute of Optoelectronics, Peking University, Nantong, Jiangsu 226010, P.R. China; Collaborative Innovation Center of Extreme Optics, Shanxi University, Taiyuan, Shanxi 030006, P.R. China*; Email: xiaoyonghu@pku.edu.cn

Hiroaki Misawa − *Research Institute for Electronic Science, Hokkaido University, Sapporo 001-0021, Japan; Center for Emergent Functional Matter Science, National Yang Ming Chiao Tung University, Hsinchu 30010, Taiwan;* orcid.org/0000-0003-1070-387X; Email: misawa@es.hokudai.ac.jp

Authors

Qiuchen Yan − *State Key Laboratory for Mesoscopic Physics and Department of Physics, Collaborative Innovation Center of Quantum Matter and Frontiers Science Center for Nano-optoelectronics, Beijing Academy of Quantum Information Sciences, Peking University, Beijing 100871, P.R. China; Research Institute for Electronic Science, Hokkaido University, Sapporo 001-0021, Japan*

En Cao − *Research Institute for Electronic Science, Hokkaido University, Sapporo 001-0021, Japan*

Yutian Ao − *State Key Laboratory for Mesoscopic Physics and Department of Physics, Collaborative Innovation Center of Quantum Matter and Frontiers Science Center for Nano-optoelectronics, Beijing Academy of Quantum Information Sciences, Peking University, Beijing 100871, P.R. China*

Xu Shi − *Creative Research Institution, Hokkaido University, Sapporo 001-0021, Japan;* orcid.org/0000-0002-6353-5470

Qihuang Gong − *State Key Laboratory for Mesoscopic Physics and Department of Physics, Collaborative Innovation Center of Quantum Matter and Frontiers Science Center for Nano-optoelectronics, Beijing Academy of Quantum Information Sciences, Peking University, Beijing 100871, P.R. China; Yangtze Delta Institute of Optoelectronics, Peking University, Nantong, Jiangsu 226010, P.R. China; Collaborative Innovation Center of Extreme Optics, Shanxi University, Taiyuan, Shanxi 030006, P.R. China*

https://doi.org/10.1021/acs.nanolett.1c03324
Nano Lett. XXXX, XXX, XXX−XXX

Complete contact information is available at:
https://pubs.acs.org/10.1021/acs.nanolett.1c03324

Author Contributions

H.M., X.H., Q.S., and Q.G. supervised the project. Q.Y. performed all of the experimental and theoretical work. E.C. and X.S. participated in the TR-PEEM measurement. Y.A. participated in discussions to the theoretical understanding of topological edge states in plasmonic nanochains. All of the authors contributed to the scientific discussions and manuscript revisions.

Notes

The authors declare no competing financial interest.

■ ACKNOWLEDGMENTS

This work was supported by the National Key Research and Development Program of China under Grants 2018YFB2200403 and 2018YFA0704404, the National Natural Science Foundation of China under Grants 61775003, 11734001, 91950204, and 11527901. We also acknowledge the financial support from JSPS KAKENHI (Grant Nos. JP18H05205 and JP20K15113), the Nanotechnology Platform (Hokkaido University), and the Dynamic Alliance for Open Innovation Bridging Human, Environment and Materials (Five-Star Alliance) of MEXT.

■ REFERENCES

(1) Lu, L.; Joannopoulos, J. D.; Soljacic, M. Topological photonics. *Nat. Photonics* **2014**, *8* (11), 821−829.
(2) Ao, Y. T.; Hu, X. Y.; You, Y. L.; Lu, C. C.; Fu, Y. L.; Wang, X. Y.; Gong, Q. H. Topological Phase Transition in the Non-Hermitian Coupled Resonator Array. *Phys. Rev. Lett.* **2020**, *125* (1), 013902.
(3) Mittal, S.; Goldschmidt, E. A.; Hafezi, M. A topological source of quantum light. *Nature* **2018**, *561* (7724), 502−506.
(4) Yang, Y. H.; Gao, Z.; Xue, H. R.; Zhang, L.; He, M. J.; Yang, Z. J.; Singh, R.; Chong, Y. D.; Zhang, B. L.; Chen, H. S. Realization of a three-dimensional photonic topological insulator. *Nature* **2019**, *565* (7741), 622−626.
(5) Liu, W. J.; Hwang, M.; Ji, Z. R.; Wang, Y. H.; Modi, G.; Agarwal, R. Z(2) Photonic Topological Insulators in the Visible Wavelength Range for Robust Nanoscale Photonics. *Nano Lett.* **2020**, *20* (2), 1329−1335.
(6) He, L.; Addison, Z.; Mele, E. J.; Zhen, B. Quadrupole topological photonic crystals. *Nat. Commun.* **2020**, *11* (1), 3119.
(7) Hafezi, M.; Demler, E. A.; Lukin, M. D.; Taylor, J. M. Robust optical delay lines with topological protection. *Nat. Phys.* **2011**, *7* (11), 907−912.
(8) Yang, B.; Bi, Y.; Zhang, R.-X.; Zhang, R.-Y.; You, O.; Zhu, Z.; Feng, J.; Sun, H.; Chan, C. T.; Liu, C.-X.; Zhang, S. Momentum space toroidal moment in a photonic metamaterial. *Nat. Commun.* **2021**, *12* (1), 1784.
(9) Bandres, M. A.; Wittek, S.; Harari, G.; Parto, M.; Ren, J. H.; Segev, M.; Christodoulides, D. N.; Khajavilchan, M. Topological insulator laser: Experiments. *Science* **2018**, *359* (6381), eaar4005.
(10) Harari, G.; Bandres, M. A.; Lumer, Y.; Rechtsman, M. C.; Chong, Y. D.; Khajavikhan, M.; Christodoulides, D. N.; Segev, M. Topological insulator laser: Theory. *Science* **2018**, *359* (6381), eaar4003.
(11) Barik, S.; Karasahin, A.; Flower, C.; Cai, T.; Miyake, H.; DeGottardi, W.; Hafezi, M.; Waks, E. A topological quantum optics interface. *Science* **2018**, *359* (6376), 666−668.
(12) Garcia-Meca, C.; Ortiz, A. M.; Saez, R. L. Supersymmetry in the time domain and its applications in optics. *Nat. Commun.* **2020**, *11* (1), 813.
(13) Fang, K. J.; Yu, Z. F.; Fan, S. H. Photonic Aharonov-Bohm Effect Based on Dynamic Modulation. *Phys. Rev. Lett.* **2012**, *108* (15), 153901.
(14) Engelhardt, G.; Benito, M.; Platero, G.; Brandes, T. Topologically Enforced Bifurcations in Superconducting Circuits. *Phys. Rev. Lett.* **2017**, *118* (19), 197702.
(15) Chaunsali, R.; Xu, H. T.; Yang, J. Y.; Kevrekidis, P. G.; Theocharis, G. Stability of topological edge states under strong nonlinear effects. *Phys. Rev. B: Condens. Matter Mater. Phys.* **2021**, *103* (2), 024106.
(16) Wang, Y. H.; Liu, W. J.; Ji, Z. R.; Modi, G.; Hwang, M.; Agarwal, R. Coherent Interactions in One-Dimensional Topological Photonic Systems and Their Applications in All-Optical Logic Operation. *Nano Lett.* **2020**, *20* (12), 8796−8802.
(17) Lustig, E.; Sharabi, Y.; Segev, M. Topological aspects of photonic time crystals. *Optica* **2018**, *5* (11), 1390−1395.
(18) Goldman, N.; Dalibard, J.; Dauphin, A.; Gerbier, F.; Lewenstein, M.; Zoller, P.; Spielman, I. B. Direct imaging of topological edge states in cold-atom systems. *Proc. Natl. Acad. Sci. U. S. A.* **2013**, *110* (17), 6736−6741.
(19) Hofmann, D.; Sentef, M. A. Resonant laser excitation and time-domain imaging of chiral topological polariton edge states. *Phys. Rev. Res.* **2020**, *2* (3), 033386.
(20) Sinev, I. S.; Mukhin, I. S.; Slobozhanyuk, A. P.; Poddubny, A. N.; Miroshnichenko, A. E.; Samusev, A. K.; Kivshar, Y. S. Mapping plasmonic topological states at the nanoscale. *Nanoscale* **2015**, *7* (28), 11904−11908.
(21) Maier, S. A.; Kik, P. G.; Atwater, H. A. Observation of coupled plasmon-polariton modes in Au nanoparticle chain waveguides of different lengths: Estimation of waveguide loss. *Appl. Phys. Lett.* **2002**, *81* (9), 1714−1716.
(22) Maier, S. A.; Kik, P. G.; Atwater, H. A. Optical pulse propagation in metal nanoparticle chain waveguides. *Phys. Rev. B: Condens. Matter Mater. Phys.* **2003**, *67* (20), 205402.
(23) Maier, S. A.; Kik, P. G.; Atwater, H. A.; Meltzer, S.; Harel, E.; Koel, B. E.; Requicha, A. A. G. Local detection of electromagnetic energy transport below the diffraction limit in metal nanoparticle plasmon waveguides. *Nat. Mater.* **2003**, *2* (4), 229−232.
(24) Brongersma, M. L.; Hartman, J. W.; Atwater, H. A. Electromagnetic energy transfer and switching in nanoparticle chain arrays below the diffraction limit. *Phys. Rev. B: Condens. Matter Mater. Phys.* **2000**, *62* (24), R16356.
(25) Sun, Q.; Yu, H.; Ueno, K.; Zu, S.; Matsuo, Y.; Misawa, H. Revealing the plasmon coupling in gold nanochains directly from the near field. *Opto-Electron. Adv.* **2019**, *2* (4), 18003001.
(26) Downing, C. A.; Weick, G. Topological collective plasmons in bipartite chains of metallic nanoparticles. *Phys. Rev. B: Condens. Matter Mater. Phys.* **2017**, *95* (12), 125426.
(27) Pocock, S. R.; Xiao, X. F.; Huidobro, P. A.; Giannini, V. Topological Plasmonic Chain with Retardation and Radiative Effects. *ACS Photonics* **2018**, *5* (6), 2271−2279.
(28) Avalos-Ovando, O.; Besteiro, L. V.; Wang, Z. M.; Govorov, A. O. Temporal plasmonics: Fano and Rabi regimes in the time domain in metal nanostructures. *Nanophotonics* **2020**, *9* (11), 3587−3595.
(29) Ueno, K.; Yang, J. H.; Sun, Q.; Aoyo, D.; Yu, H.; Oshikiri, T.; Kubo, A.; Matsuo, Y.; Gong, Q. H.; Misawa, H. Control of plasmon dephasing time using stacked nanogap gold structures for strong near-field enhancement. *Appl. Mater. Today* **2019**, *14*, 159−165.
(30) Li, Y. L.; Sun, Q.; Zu, S.; Shi, X.; Liu, Y. Q.; Hu, X. Y.; Ueno, K.; Gong, Q. H.; Misawa, H. Correlation between Near-Field Enhancement and Dephasing Time in Plasmonic Dimers. *Phys. Rev. Lett.* **2020**, *124* (16), 163901.
(31) Asbóth, J. K.; Oroszlány, L.; Pályi, A. A short course on topological insulators. *Lecture notes in physics*; Springer: 2016; Vol. *919*, pp 997−1000.
(32) Romero, I.; Aizpurua, J.; Bryant, G. W.; Garcia De Abajo, F. J. Plasmons in nearly touching metallic nanoparticles: singular response in the limit of touching dimers. *Opt. Express* **2006**, *14* (21), 9988−9999.

(33) Sun, Q.; Zu, S.; Misawa, H. Ultrafast photoemission electron microscopy: Capability and potential in probing plasmonic nanostructures from multiple domains. *J. Chem. Phys.* **2020**, *153* (12), 120902.
(34) Shi, X.; Ueno, K.; Oshikiri, T.; Sun, Q.; Sasaki, K.; Misawa, H. Enhanced water splitting under modal strong coupling conditions. *Nat. Nanotechnol.* **2018**, *13* (10), 953−958.
(35) Yang, J. H.; Sun, Q.; Ueno, K.; Shi, X.; Oshikiri, T.; Misawa, H.; Gong, Q. H. Manipulation of the dephasing time by strong coupling between localized and propagating surface plasmon modes. *Nat. Commun.* **2018**, *9*, 4858.
(36) Wokaun, A.; Gordon, J. P.; Liao, P. F. Radiation damping in surface-enhanced raman-scattering. *Phys. Rev. Lett.* **1982**, *48*, 1574.
(37) Lamprecht, B.; Leitner, A.; Aussenegg, F. R. SHG studies of plasmon dephasing in nanoparticles. *Appl. Phys. B: Lasers Opt.* **1999**, *68*, 419.

https://doi.org/10.1021/acs.nanolett.1c03324
Nano Lett. XXXX, XXX, XXX−XXX